SOFTWARE-BASED CHARGE DEEP LEVEL TRANSIENT SPECTROMETER FOR THE CHARACTERIZATION OF SEMICONDUCTOR MATERIALS

Daniel E. MONTENEGRO[a] Jason B. ROTHENBERGER Mark A. PRELAS
Tushar K. GHOSH Robert V. TOMPSON Sudarshan K. LOYALKA
Nuclear Science and Engineering Institute, University of Missouri, Columbia, Missouri
[a] demq53@mail.missouri.edu

Abstract: *Presented is a software-based Charge Deep Level Transient Spectroscopy system (Q-DLTS) for the characterization of semiconductor materials. The design innovation lies in the exclusion of all hardware-based data processing in favor of upgradable software-based algorithms. The only essential electronic hardware is that needed to amplify and integrate the thermally emitted trapped charge transients, and to provide the timing signals that control each measurement cycle. The data acquisition device samples the amplified charge output at a user-defined sampling rate, and then transfers the digitized data to the computer's memory. The software algorithm then digitally compensates for spurious input signals and filters the raw data to produce a Q-DLTS spectrum based upon user-defined input parameters. The software implementation of a conventional DLTS double boxcar algorithm is described. The device was benchmarked by monitoring deep-level traps present in blue GaN/SiC light-emitting diodes and to establish the presence of a minority-carrier trap occurring at a discrete energy below the conduction band with an apparent activation energy E_a = 0.381 eV, a capture cross-section $\sigma = 1.69 \times 10^{-17}$ cm^2, and a maximum total charge output of Q_0 = 2.99 pC at T = 297 K. These values are consistent with those of a deep donor originating from a nitrogen vacancy defect.*

Key words: *DLTS, LEDs, GaN, SiC, semiconductors.*

1. Introduction.

One of the most common methods for the characterization of deep-level centers in semiconductors is Deep-Level Transient Spectroscopy (DLTS) [1]. First described by Lang [2], this technique is based on the measurement of junction capacitance transients due to the thermal emission of a deep level's carrier population as it returns to equilibrium. However, conventional DLTS suffers from inherent limitations. Capacitance spectroscopy typically exhibits poor sensitivity or heavily doped materials [3]. For wide bandgap semi-insulating materials that exhibit large series resistance, the capacitance transients may be too slow for the measurement frequency [4]. Furthermore, systems that use a capacitance bridge for measurement are slow, which limits its usable range to traps above an activation energy of 0.1 eV [5]. Commercially available systems usually rely on hardware-based timing mechanisms to perform the required DLTS signal processing. Alternative measurement schemes have been proposed over the years. Some of these methods rely on the direct measurement of thermally stimulated current transients or–as in the present work–the integration of these currents to yield charge transients (Q-DLTS) [7-8].

Presented in this work is a software-based Charge Deep Level Transient Spectroscopy system that is both portable and relatively easy to construct. Recently, this instrument was used to characterize the surface charge states of single crystal Aluminum Nitride (AlN) induced by adsorbed vapor molecules in the environment [9].

2. Theory

Similar to Lang's original dual-gated signal averaging or double boxcar DLTS method, the Q-DLTS technique relies on cyclic bias pulses to momentarily excite the traps of p-n junctions and Schottky barriers. The electron occupation of a level is monitored as it returns to thermal equilibrium by measuring the associated charge transients. In this scheme, a rate window is defined as a function of two measuring gate times (t_1 and t_2) starting at the beginning of the trap discharge. The charge transient is measured at these two times and the difference, $Q(t_2)–Q(t_1)$, is plotted as a function of temperature. According to Maxwell-Boltzmann statistics, the thermal emission rates are strongly dependent upon temperature. At a particular temperature, a thermal scan will produce an emission rate that matches the rate window. Therefore, a peak in the spectrum occurs because $Q(t_2)–Q(t_1)$ is maximized. If several emission rates are present then multiple peaks will emerge.

If the time-dependent trap distribution is assumed to be uniform then the current can be described as [7],

$$i(t) = \frac{AqWN_T \exp\left(\frac{-t}{\tau_T}\right)}{2\tau_T} \quad (1)$$

where A is the junction area, q is the elementary charge, W is the junction depletion width, N_T is the trap density, and τ_T is the trap decay time constant. To

obtain the charge emitted, the previous equation must be integrated over time,

$$Q(t)=\int_0^t i(t)\,dt=\frac{AqWN_T}{2\tau_T}\int_o^t \exp\left(-\frac{t}{\tau_T}\right)dt= \frac{AqWN_T}{2}\left(1-\exp\left(-\frac{t}{\tau_T}\right)\right) \quad (2)$$

The prefactor in Eq. (2) is the total charge collected:

$$Q_0=\int_0^\infty i(t)\,dt=\frac{AqWN_T}{2} \quad (3)$$

Traditionally in DLTS, the rate window or τ^{-1} is kept constant while the temperature is varied. A similar method is to maintain a constant temperature while the rate window is varied [8]. This rate window can be described as a function of the ratio of the gate times (i.e., $t_2/t_1=\alpha$) as

$$\tau^{-1}=\frac{\ln(t_2/t_1)}{t_2-t_1}=\frac{\ln\alpha}{(\alpha-1)t_1} \quad (4)$$

Also similar to Lang's algorithm, the gate timed charge difference emitted from the beginning of discharge is simply,

$$\Delta Q=Q(t_1)-Q(t_2) \quad (5)$$

For electrons, the previous equation can be also written as,

$$\Delta Q=Q_0\left(\exp(-e_n t_1)-\exp(-e_n t_2)\right) \quad (6)$$

where e_n is the electron emission rate, which has the form [10],

$$e_n=\sigma\Gamma_n T_S^{\,2}\exp\left(-\frac{E_a}{kT_S}\right) \quad (7)$$

where σ is the capture cross-section, T is the temperature, E_a is the activation energy, k is the Boltzmann constant, and Γ_n is defined as,

$$\Gamma_n=2\sqrt{3}\left(2\pi/h^2\right)^{3/2}k^2 m_n \quad (8)$$

where h is Planck's constant and m_n is the effective mass of the electron. The equations for holes are analogous. For a given temperature, a maximum in the spectrum will occur when the rate window equals the emission rate of the trap. This can be easily verified by differentiating Eq. (6), which yields,

$$\tau_t^{-1}=e_n=\frac{\ln\alpha}{(\alpha-1)t_1}=\tau^{-1} \quad (9)$$

Substituting for α=2 into Eq. (9) we have,

$$e_n=\ln 2/t_1 \quad (10)$$

Substituting this value back into Eq. (6) we obtain,

$$\Delta Q_{\max}=Q_0/4 \quad (11)$$

This last equation allows a direct calculation of the total charge collected from the Q-DLTS peak maxima. The value of α (i.e., t_2/t_1) can vary; however, in the present design α = 2 since it is a standard value found elsewhere the literature [11]. Because of the Arrhenius dependence of the emission rate, the values of σ and E_a can be calculated using Eq. (7). Although not investigated in this paper, other averaging algorithms such as nth-Order Filtering, Fourier-based Multi-Exponential DLTS and the Gardner transform are possible [12-14]. These alternative algorithms can complement the poor energy resolution shown by the standard double boxcar method [15]. Finally, the deep-level density (N_T) can be calculated using Eqs. (3) and (11) as,

$$N_T=\frac{2Q_0}{AqW} \quad (12)$$

3. Circuit Design.

Fig. 1 is a diagram of the current integration circuit used to obtain the charge output of the device under test (DUT). The integrator operational amplifier is an ultra-low current amplifier (≈ 25 fA maximum input current). The input bias current of the device can be compensated with a simple voltage divider circuit. For proper circuit behavior leakage currents must be controlled; especially at low input currents. If care is taken with the hardware component arrangement, and correction algorithms are employed to overcome non-ideal circuit behavior (i.e., charge injection, parasitic capacitive coupling, electronic noise, etc.) then the sensitivity range of the system can be extended into the femto-coulomb (fC) region.

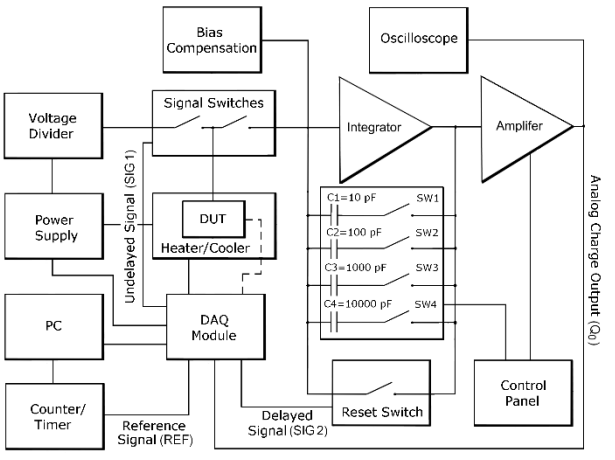

Figure 1. Integrating and amplifying electrical circuit diagram

The switching mechanism (i.e., signal and reset switches) needs to be fast enough that the fast thermal emptying transients (> 10 μs) can be sampled without signal degradation. Experiments with electromechanical relays were unsuccessful due to the large commutation noise and slow operating

times. Solid-state analog switches based on CMOS technology with sub-picoamp leakage currents (≈ 0.1 pA) and low charge injection (≈ 2 pC) proved more successful. This type of switch was also used for the integrator reset switch that controls the sampling/integration cycle (T) and delay time (t_d).

If the DUT is a p-n or Schottky diode, then a reverse bias or quiescent voltage (V_B) is needed during the relaxation part of the measurement cycle. In this "Series Mode", the leftmost signal switch (see Fig. 1) is kept open, and the filling voltage (ΔV_B) is generated from one of the built-in analog outputs of the Data Acquisition (DAQ) Device [16]. This analog waveform must be externally triggered by a Reference Signal (REF in Fig. 2), and offset by V_B during the relaxation part of the measurement cycle. The analog bias pulse width (t_c) is then configured to have the same length as the delayed switching signal (i.e., $t_c = t_f + t_d$, where t_d is the delay time and t_f is the bias pulse width). As in Lang's DLTS method, two types of momentary filling, or bias, pulses are possible, a saturating injection or forward bias pulse, which injects minority carriers into the depletion region, and a majority carrier or reverse bias pulse, which introduces majority carriers into the depletion region [2].

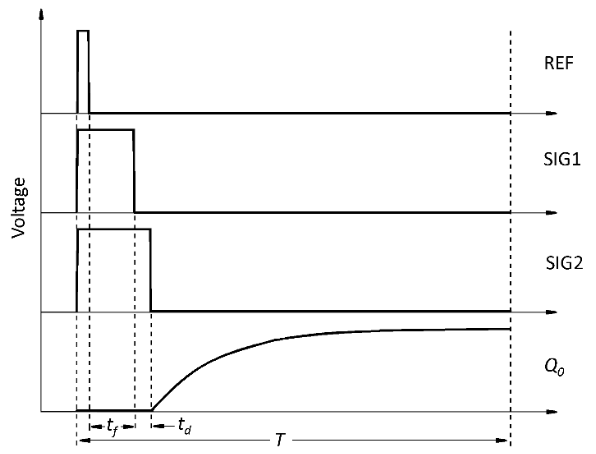

Figure 2. Timing waveform diagram showing the three counter/timer signals and a simplified exponential integrator output signal during a single measuring cycle. The top three waveforms are the voltage signals that control the switching, and Q_0 is a representative integrator output. T is the period of a single measurement cycle. Graph not to scale.

In "Parallel Mode", ΔV_B can be provided solely by the voltage divider shown in Fig. 1. This configuration was designed for semiconductor-based sensors with symmetrical electrodes deposited on the sensing surface [5, 9]. A light pulse is an effective mode of deep-level states' excitation that is particularly well suited for this configuration; this technique is called Photoinduced Current Transient Spectrometry or PICTS [17].

4. Timing Signals

Three counters/timers are needed to produce the timing signals. The reference signal controls the period of the excitation/discharge cycle. The period must be long enough for all the long-lived trapped charge transients to decay away. This can be done by visually checking—with an oscilloscope or a recurrent voltage vs. time plot—for a flattening or plateauing of the total charge collected, and ensuring that the next cycle starts at some point in this region. In the present design, the REF signal is obtained via a counter/timer based on a CTS 9513 Timing Controller chip, which has five independent 16-bit counters (i.e., 65,536 maximum counts). Two additional 32-bit counter/timers were used to generate un-delayed and delayed switching signals (i.e., SIG1 and SIG2 respectively) using the period pulse signal as a trigger source. The adjustable delay (t_d) of SIG2 must be added to avoid the integration of the aforementioned switching transients. The three timing and switching signals (i.e., REF, SIG1 and SIG2) must be produced continuously until all sampling cycles are completed and the sampled data is stored.

5. Data Acquisition

The analog-to-digital (A/D) conversion and timing section flowchart is shown in Fig. 3. The program first configures the task of producing the charge/discharge cycle trigger pulse train (i.e., the REF waveform). After this, the DAQ device digitizer counting tasks are initialized and configured.

The sampling rate of the de-excitation transient must be fast enough that even fast thermal emissions can be processed by the Q-DLTS algorithm. This can only be accomplished if the sampling rate (f_s) and the initial and final values of the rate window array (τ_0 and τ_f, respectively) obey two constraint equations. The first equation is,

$$f_s^{-1} \geq \ln\alpha\left(\left(10\wedge\left(\log\tau_0 + I\right)\right) - \left(10\wedge\left(\log\tau_0\right)\right)\right) \tag{14}$$

where I is the logarithmic rate window interval defined by,

$$I = \frac{\log(\tau_0) - \log(\tau_f)}{n} \tag{15}$$

and n is the desired number of points on the abscissa of the Q-DLTS spectrum.

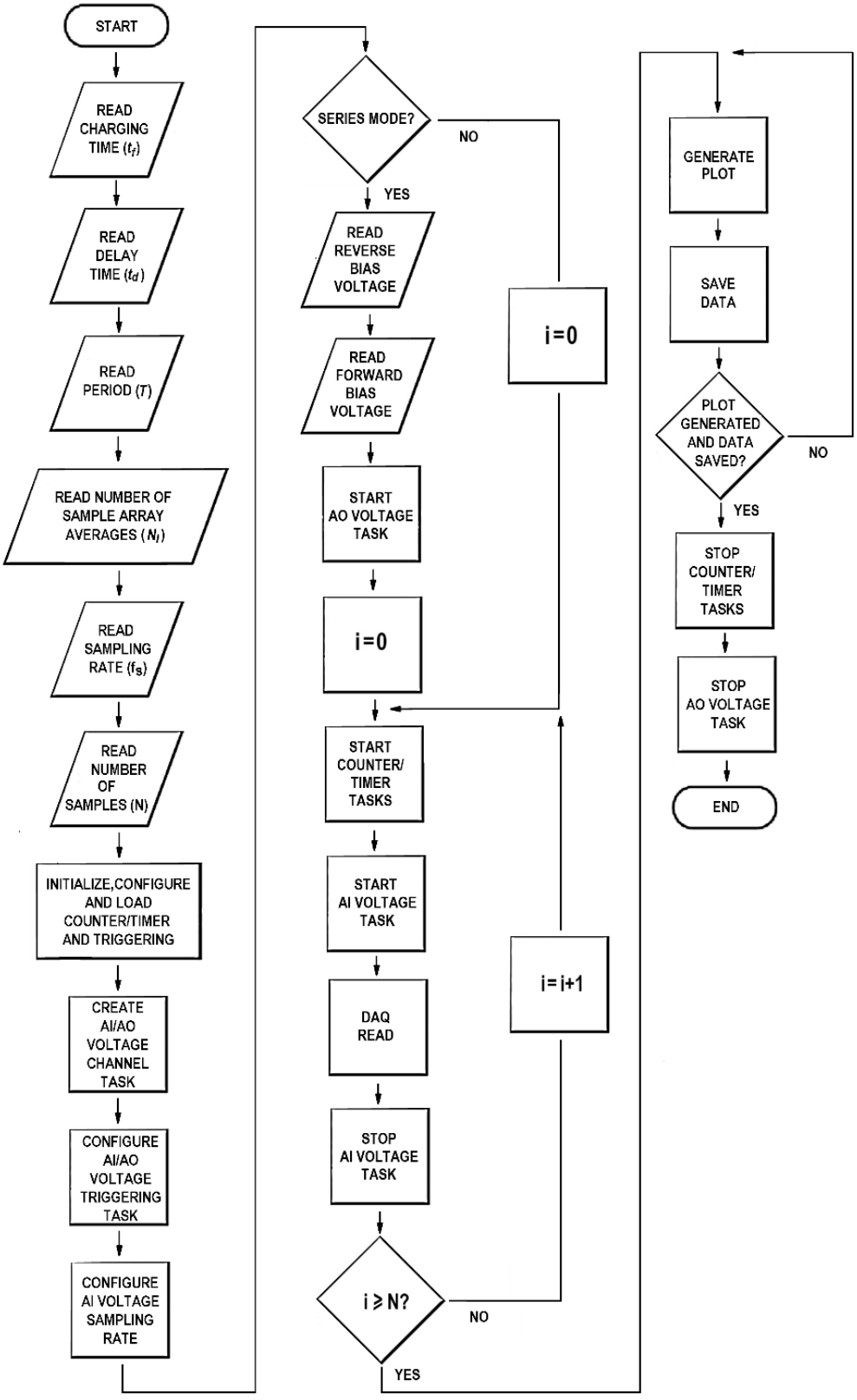

Figure 3. Simplified flowchart of the sampling and timing control algorithm

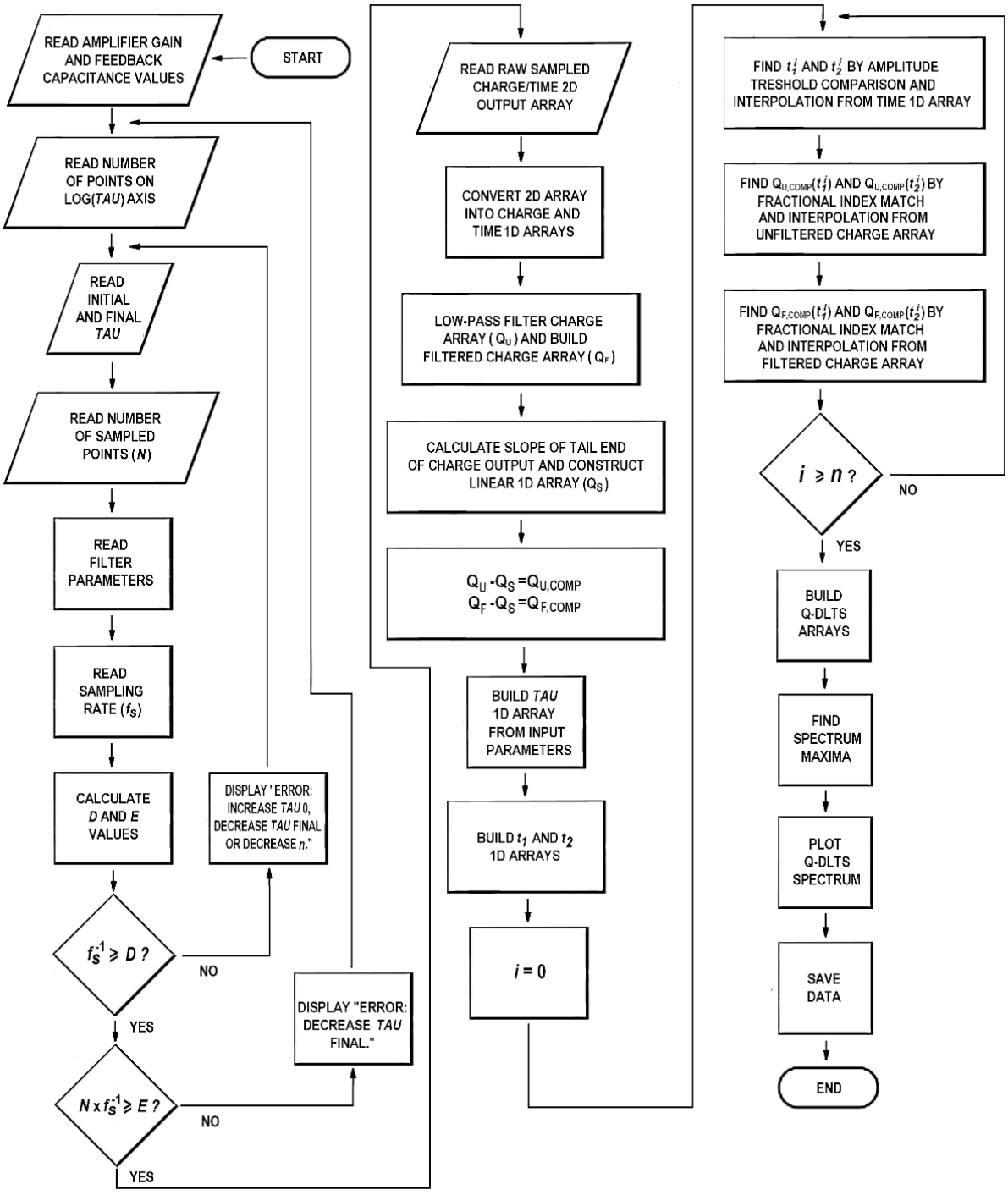

Figure 4. Simplified flowchart of the Q-DLTS program showing the modified double boxcar algorithm.

Each value of the rate window array can be calculated with the following equation,

$$\tau_i = 10\wedge\left(\log\left(\tau_0\right)+iI\right) \quad (16)$$

It is easy to verify that the subtraction terms of Eq. (14) correspond to τ_1 and τ_0, respectively.

Because we are dealing with discrete values, the inverse of the sampling rate cannot be lesser than the difference of the first two user-selected values of t_1. For simplicity, the right-hand side of Eq. (14) is named *D* in the flowchart of Fig. 4. The second constraint equation is

$$Nf_s^{-1} \geq \alpha \ln\left(\alpha\right)\tau_f \quad (17)$$

where *N* is the total number of sampled points. The right -hand side of Eq. (17) corresponds to the largest value of t_2, forcing this value not to exceed the last sampled data point. Since extrapolation is unfeasible at these ranges, the highest rate window and its associated t_2 value account for the majority of redundant data. For simplicity, the numerator of the right-hand side of Eq. (17) is named *E* in the flowchart of Fig. 4.

The DAQ device's Analog Input (AI) task is set up by creating an analog input channel to measure voltage. Then, the user-defined sampling rate is configured by setting the source of the sample clock. Finally, the triggering for the task is configured to use the delayed switching signal (SIG2) as a trigger source. The start, read and stop parameters of the task are located inside a loop. Similar steps are performed for the Analog Output (AO) task. Each filling pulse is associated with a unique transient decay curve that is averaged after each cycle. The resulting data is stored in an array that is carried from an iteration to the next via shift registers. The effect of electromagnetic interference can be significantly diminished by increasing the number of iterations (N_I). After a preset number of iterations is reached, the averaged data array is stored and a plot is generated. An oscilloscope can be used for qualitative purposes such as the visual inspection of the shape of the raw DUT charge output.

During data acquisition, the software host communicates with the digitizer via a single Universal Serial Bus (USB) port. To ensure high-speed bidirectional analog data transfer over USB, the data acquisition is hardware-timed and buffered by means of a First In/First Out (FIFO) integrated circuit.

6. Q-DLTS Algorithm

The program illustrated in Fig. 4 essentially executes the double boxcar algorithm and other essential parameter calculations such as the number of abscissa (τ-axis) data points. The parameter input sequence is inside a loop structure to ensure that the sampling rate constraints of Eqs. (14) and (17) are met; if this is not achieved, the program prompts the user to reenter valid input values.

The amplitude or charge output array is first smoothed by the mean displaced ratio (MDR) method [18] and then it is digitally filtered via a Butterworth low-pass filter. This filter was chosen due to its small frequency response characteristics but other processing filtering are possible. Knowing *I*, *n* and τ_0 allows the program to calculate each pair of t_1 and t_2 values by linear interpolation from the time array. The corresponding charge values are then linearly interpolated from the amplitude array, which was previously converted to the appropriate units of charge. Finally, the spectrum is plotted and the data is stored in the PC's memory. The Q-DLTS peaks are calculated by grouping sequential data points in arrays of equal user-defined lengths. Each group of data points are fit into quadratic polynomials and then differentiated twice to obtain each peak's amplitude, location and sharpness.

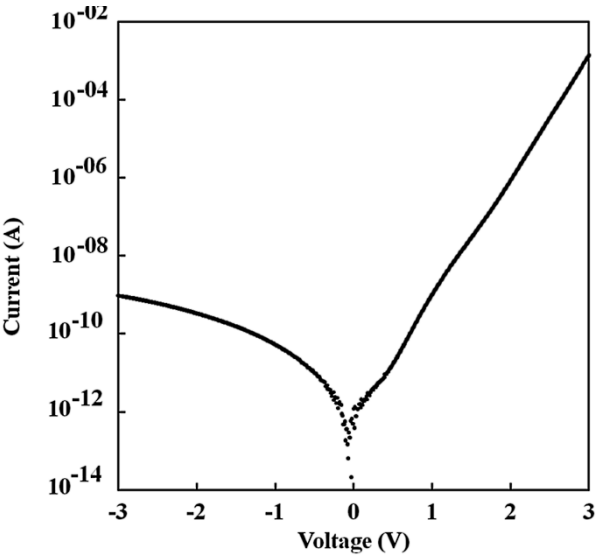

Figure 5. Room temperature I-V characteristics of the as-received GaN/SiC blue LED structure

7. Non-Ideal Behavior Compensation

A typical Q-DLTS uncompensated spectrum will show the presence of several non-ideal spectral features, most notably the junction's temperature-dependent leakage current under reverse bias. This signal is unavoidably integrated alongside the charge output of the DUT, and appears as an exponentially increasing charge output at the tail-end of the spectrum. This behavior can be partially hardware-compensated with a bias resistance as shown in Fig.1; in addition, two leakage suppression algorithms are provided. If the leakage is integrated

and digitized from a diode under reverse bias, then this data set can then be subtracted from the total charge output. An alternative algorithm is to calculate the slope of the leakage vs. time curve after all transients attributed to carrier emission have decayed away. Since the leakage is usually constant, the slope is then used to artificially create an integrated leakage current array that is subtracted from the total charge output array.

Another non-ideal spectral feature accentuated at low trap concentrations is the presence of fast isothermal narrow peaks associated with coupled parasitic capacitance and switching charge injection. For any given peak, the Q-DLTS spectrum contains information of both the total charge output of Eq. (11) and the transient time constant of Eq. (9). Therefore, these parameters can be used to artificially generate an identical charge data array to that produced by the parasitic capacitance, and subtract it from the total charge output. Finally, if the time constant of the capacitive coupling is faster than that of the fastest sampled trap then the time delay feature (t_d in Fig. 2) can be used.

8. Comparison with Similar Systems

When comparing the present apparatus to that of Arora et al. [8], it is evident that both Q-DLTS systems have similar charge collection circuit design: two fast-acting switches controlling the charge-discharge timing located at the input stage between the Device Under Test (DUT), a trap excitation circuit, an integrating amplifier and a second-stage linear amplifier. Both systems perform the same DLTS filtering based on Lang's dual-gated signal averager or double boxcar algorithm in which the rate window is kept fixed while the DUT temperature is scanned to obtain different capacitance or charge transients. A notable difference between the two systems, however, is the realization of double boxcar averaging. Most prior designs relied on a sample-and-hold circuit to perform the double boxcar averaging but it allowed no straightforward way to implement modifications to overcome the inherent limitations of the DLTS.

Previous computer-based systems that performed such functions, such as that of Doolittle and Rohatgi [19], relied on a time-saving pseudo-logarithmic sampling algorithm that avoided oversampling of non-relevant data by reusing the data contained within the faster sampling rates. The configuration described in the present work allows the use of a fixed sampling rate per transient and relinquishes all data manipulation, including the DLTS algorithm, to the post-sampling filtering software.

9. Benchmarking

The apparatus was benchmarked using commercially-available low-brightness GaN on SiC blue light-emitting diodes (LEDs) [20]. Group-III nitrides LED structures have been extensively studied in the past in terms of failure modes, degradation and aging mechanisms [21-23], and thus are well suited for benchmarking purposes. The photoluminescence in the blue spectral range is obtained by the incorporation of Mg acceptor impurities, which results in *p*-type doping [24]. Nitrogen vacancies (V_N) are also formed during the GaN growth with similar concentrations of that of the Mg acceptor [25].

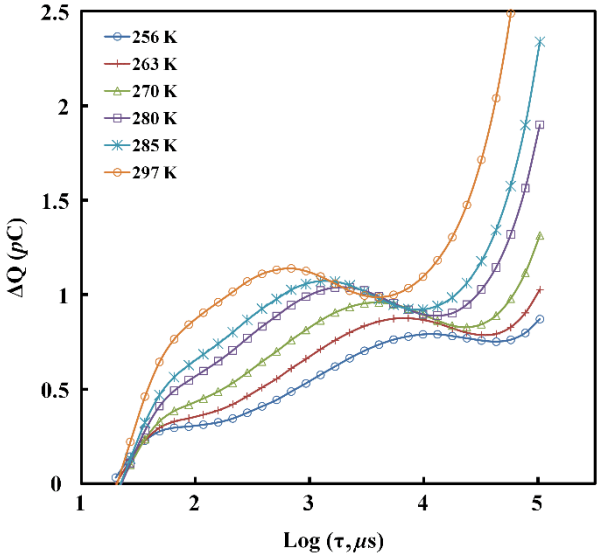

Figure 6. Uncompensated Q-DLTS spectra showing typical artifacts caused by leakage currents and parasitic capacitance.

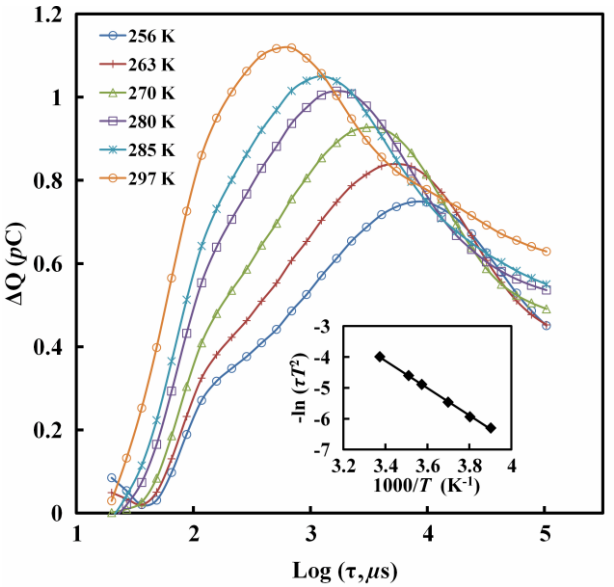

Figure 7. Compensated Q-DLTS spectra obtained from the as-received sample. Inset: Arrhenius plot showing the trap signature with an activation energy E_a = 0.381 eV, and a capture cross-section σ = 1.69 x 10^{-17} cm^2.

The LED structures under test were of the form of square dices (0.0136 x 0.0136 mm^2) mounted *p*-side

up on ceramic stems and encapsulated in epoxy resin. In the present study, four LED junctions were connected in parallel to increase the deep centers' charge output [22].

Q-DLTS measurements were carried out using the following parameter values: ΔV_B = 3.5 V, V_B = -1.0 V, t_c = 20 ms, td = 0 μs, T = 200 ms, N_I = 100, A_v = 226 dB, and f_s = 250 kHz. This particular saturating injection pulse voltage, which matches the GaN bandgap, was chosen to reveal the minority-carrier traps (i.e., donor levels) present in the structure. The measurements were performed in increments of ≈ 7 K over a temperature range of 256–296 K.

10. Results and Discussion

The characteristic I-V curve of the as-received sample at room temperature (Fig. 5) confirms the presence of a p-n junction. Fig. 6 shows the uncompensated Q-DLTS spectrum of the as-received LED device. The graph shows the presence of a typical isothermal capacitance peak at $\tau \approx 50$ μs; however, its small amplitude does not interfere with the measurement of the main peak under test. Leakage effects, on the other hand, are significant and must be compensated (see Fig. 7) before data transferal to the peak-finding algorithm previously described.

As shown in Table 1, the trap parameters obtained with the present system closely match those found in the literature for similar LED structures but utilizing standard capacitance DLTS methods. In particular, a state of similar activation energy has previously been associated to a deep Mg-V_N donor center formed when an Mg acceptor associates with an oppositely charged nearest-neighbor nitrogen vacancy in the case of high Mg doping levels [27]. This complex, together with a Mg shallow acceptor, participate in a Donor-Acceptor Pair (DAP) transition that has been shown to be responsible for the well-documented 2.8 eV blue photo-luminescence band at room temperature [25].

Table 1. Literature comparison of the electrical properties of GaN-based Blue LEDs. Only deep-level parameters associated with unstressed and unaged samples are listed.

Energy (eV)	Capture cross section (cm^2)	Type	Method used	Source
0.38	3.90×10^{-16}	N/A	DLTS	Menghesso *et al.*[21]
0.180, 0.180, 0.170	9×10^{-14}, 5×10^{-19}, 1×10^{-20}	both	DLTS	Rossi *et al.*[26]
0.350–0.430	N/A	donor	Photoluminescence	Qu *et al.*[27]
0.381	1.69×10^{-17}	donor	Q-DLTS	Present work.

11. Conclusions

A simple software-based Q-DLTS instrument and method to characterize the surface and bulk deep states in semiconductor materials was described. The novelty of the design lies in its modularity capabilities, high sensitivity and simplicity. Its construction only requires a low-noise integration amplifier circuit with fast switching capabilities, a high-speed DAQ device, three counter/timers, and a PC running a suitable programming language. With this instrument, the user has full data control and visualization during all stages of measurement; from the initial post-sampling to the final Q-DLTS spectrum. All the required constraint and sampling parameters, error analysis and programming details were described.

An essential component of the system is the software-based Q-DLTS algorithm. In previous works, this algorithm has been implemented by hardware components, or by more complicated pseudo-logarithmic storage schemes. In the present work, the dual-gated signal averaging, the compensation for non-ideal circuit behavior and other data manipulation are performed post-sampling by the software. This does not translate into longer processing times because the time spent by traditional DLTS hardware circuits in repetitive measurement cycles of increasing length is entirely avoided. Instead, the algorithm speedily obtains the desired emission spectrum based on user-defined parameters.

The device described in this work was used to study the deep-levels present in commercial GaN blue LEDs. The sample temperature range was 256–296 K. A single deep-level was found, with an apparent activation energy E_a = 0.381 eV and capture cross-section $\sigma = 1.69 \times 10^{-17}$ cm^2. This energy level is consistent with reported values.

References

1. Bozyigit, D., Jakob, M., Yarema, O., Wood V., Deep Level Transient Spectroscopy (DLTS) on Colloidal-Synthesized Nanocrystal Solids. In: Appl. Mater.

Interfaces, 5 (2013), No. 8, March 2013, pp. 2915-2919.
2. Lang, D.V.: *Deep-level transient spectroscopy: A new method to characterize traps in semiconductors*. In: J. Appl. Phys., 45 (1974), No.7, July 1974, pp. 3023-3032.
3. Miller, G.L., Lang, D.V. and Kimerling, L.C.: *Capacitance Transient Spectroscopy*. In: Ann. Rev. Mater. Sci., 7, (1977), August 1997, pp. 377-448.
4. Nadazy, V., Durny, R., and Pincik, E.: *Evidence for the Improved Defect-Pool Model for Gap States in Amorphous Silicon from Charge DLTS Experiments on Undoped a-Si:H*. In: Phys. Rev. Lett., 78 (1997), No.6, February 1997, pp. 1102-1105.
5. Kachwalla, Z. and Miller, D.J.: *Transient spectroscopy using the Hall Effect*. In: Appl. Phys. Lett., 50 (1987) No.20, May 1987, pp. 1438-1440.
6. Kirov, K.I., and Radev, K.B.: *A simple charge-based DLTS technique*. In: Phys. Stat. Sol. A, 63 (1981), No.2, February 1981, pp. 711-716.
7. Farmer, J.W., Lamp, C.D. and Meese, J.M.: *Charge Transient Spectroscopy*. In: Appl. Phys. Lett., 41 (1982) No.11, December 1982, pp. 1063-1065.
8. Arora, B.M., Chakravarty, S., Subramanian, S., Polyakov, V.I., Ermakov, M.G., Ermakova, O.N. and Perov, P.I.: *Deep-level transient charge spectroscopy of Sn donors in $Al_xGa_{1-x}As$*. In: J. Appl. Phys., 73 (1993), No.4, February 1993, pp. 1802-1806.
9. Rothenberger , J.B., Montenegro, D.E., Prelas, M.A, Ghosh, T.K, Tompson, R.V, and Loyalka, S.K., An Aluminum Nitride-based chemical sensor using Q-DLTS. In: Diamond Relat. Mater., 23 (2012), March 2012, pp. 72-75.
10. Polyakov, V.I., Rossukanyi, N.M., Rukovishnikov, A.I., Pimenov, S.M., Karabutov, A.V. and Konov, V.I.: *Effects of post-growth treatment and coating with ultrathin metal layers on the band bending and field electron emission of diamond films*. In: J. Appl. Phys., 84 (1998), No.5, September 1998, pp. 2882-2889.
11. Thurzo, G. P., Zahn, D. R. T., Dua, A. K., Roy, M. and George, V. C.: *The origin of charge transients in Al/undoped diamond/p-Si diodes*. In: Diamond Relat. Mater., 11 (2002), No.3-6, March-June 2002, pp. 400-404.
12. Crowell, C. R. and Alipanahi, S.: *Transient Distortion and nth Order Filtering in Deep Level Transient Spectroscopy (D^nLTS)*. In: Solid-State Electron., 24 (1981),No. 1, January 1981, pp. 25-36.
13. Morimoto, J., Kida, T., Miki, Y. and Miyakawa, T.: *Multi-Exponential Analysis of DLTS*. In: Appl. Phys. A, 39 (1986) No. 3, March 1986, pp. 197-202.
14. Gardner, D. G., Gardner, J. C., Laush, G. and Meinke, W. W.*: Method for the Analysis of Multi-Components Exponential Decays*. In: J. Chem. Phys., 31 (1959), No.4, October 1959, pp. 978-986.
15. Dobaczewski, L., Kaczor, P., Hawkins, I.D. and Peaker, A.R.: *Laplace transform deep-level transient spectroscopic studies of defects in semiconductors*. In: J. Appl. Phys., 76 (1994) No.1, July 1994, pp. 194-198.
16. USB-6221 M Series multifunction data acquisition (DAQ) module, available from National Instruments Corporation, 11500 N Mopac Expwy, Austin, TX 78759-3504, USA.
17. Tapiero, M., Benjelloun, N., Zielinger, J.P., Hamd, S.E. and Noguet, C.: *Photoinduced current transient spectroscopy in high-resistivity bulk materials: Instrumentation and methodology*. In: J. Appl. Phys., 64 (1988) No.8, October 1988, pp. 4006-4012.
18. Dyson, R.D. and Isenberg, I.: *Analysis of exponential curves by a method of moments, with special attention to sedimentation equilibrium and fluorescence decay*. In: Biochemistry, 10 (1971), 3233.
19. Doolittle, W. A. and Rohatgi, A.: *A novel computer based pseudo-logarithmic capacitance/conductance DLTS system specifically designed for transient analysis*. In: Rev. Sci. Instrum., 63 (1992), 5733.
20. KP-1608MBC blue LED, available from Kingbright Corporation, 225 Brea Canyon Road, City of Industry, CA 91789, USA.
21. Meneghesso, G., Levada, S., Pierobon, R., Rampazzo, F., Zanom, E., Cavallini, A., Castaldini, A., Scamarcio, G., Du, S. and Eliashevich, I.: *Degradation mechanisms of GaN-based LEDs after accelerated DC current aging*. In: Electron Devices Meeting, 2002, IEDM '02, International, December 8-11, 2002, San Francisco, California, pp. 103-106.
22. Zdansky, K., Zavadil, J., Nohavica, D. and Kugler, S.: *Degradation of commercial high-brightness GaP:N green light emitting diodes*. In: J. Appl. Phys., 83 (1998) No.12, June 1998, pp. 7678-7684.
23. Arslan, E., Bütün, S., Lisesivdin, S.B., Kasap, M., Ozcelik, S. and Ozbay, E.: *The persistent photoconductivity effect in AlGaN/GaN heterostructures grown on sapphire and SiC substrates*. In: J. Appl. Phys., 103 (2008), No.10, May 2008, pp. 103701-10702.
24. Smith, M., Chen, G.D., Lin, J.Y., Jiang, H.X., Salvador, A., Sverdlov, B.N., Botchkarev, A., Morkoc, H. and Goldenberg, B.: *Mechanisms of band-edge emission in Mg-doped p-type GaN*. In: Appl. Phys. Lett., 68 (1996), No.14, April 1996, pp. 1883-1885.
25. Kaufman, U., Kunzer, M., Maier, M., Obloh, H., Ramakrishnan, A., Santic, B. and Schlotter, P.: *Nature of the 2.8 eV photoluminescence band in Mg doped GaN*. In: Appl. Phys. Lett., 72 (1998), No.11, March 1998, pp. 1326-1328.
26. Rossi, F., Pavesi, M., Meneghini, M., Salviati, G., Manfredi, M., Meneghesso, G., Castaldini, A., Cavallini, A., Rigutti, L., Strass, U., Zehnder, U. and Zanoni, E.: *Influence of short-term low current dc aging on the electrical and optical properties of InGaN blue light-emitting diodes*. In: J. Appl. Phys., 99 (2006), No. 5, March 2006, pp. 053104-053105.
27. Qu, B.Z., Zhu, Q.S., Sun, H., Wan, S.K., Wang, Z. G., Nagai, H., Kawaguchi, Y., Hiramatsu, K. and Sawaki, N.: *Photoluminescence of Mg-doped GaN grown by metalorganic chemical vapor deposition*. In: J. Vac. Sci. Technol. A, 21 (2003), No.4, July 2003, pp. 838-841.